Hybrid Wide-Band Staircase Filters in Rectangular Waveguide With Enhanced Out-of-Band Response

Joaquin F. Valencia Sullca, Marco Guglielmi, *Life Fellow, IEEE,* Santiago Cogollos, *Member, IEEE* and Vicente E. Boria, *Fellow, IEEE*

***Abstract*—The objective of this paper is to describe the design of a new family of wide-band filters in rectangular waveguide based on hybrid couplings and a staircase configuration. The use of E-plane T-junctions and E-plane folded structures is also discussed, in order to enhance the out-of-band response and the selectivity of the filter with respect to the current state-of-the-art. The design of several hybrid filter prototypes is discussed in detail including also manufacturing sensitivity and high power analysis. Finally, simulations and measurements for an eight-pole filter prototype are also compared, showing very good agreement, thereby fully validating both the design procedure and the new filter topology that we propose.**

***Index Terms*—Aggressive space mapping, band-pass filters, hybrid (inductive and capacitive) irises, manifold connections, staircase configuration, wide-band response.**

I. Introduction

MODERN communication systems require hardware with small size, wide operational bandwidth, and higher power capabilities. Microwave filters, in particular, need to provide improved selectivity and higher out-of-band rejection. The out-of-band performance is, in fact, one of the key parameters in the design of a microwave filter. In this context, it is well known that the appearance of spurious responses close to the filter pass-band can be one of the most challenging issues that needs to be addressed in the design of microwave filter in rectangular waveguide technology ([1],[2]). Many approaches have indeed been developed in the past to overcome this problem. Traditionally, waveguide low-pass filters have been connected in cascade to bandpass filters in order to obtain a wide spurious-free frequency response and suppress, at the same time, all the higher order modes in the stop band, as discussed, for instance, in [3] and [4].

In this context, the inductive bandpass filter is one of the most common filter implementation in rectangular waveguide technology [5]. This is because the design of inductive filters is very well established, the fabrication cost can be very low, it has excellent high power capabilities and very good selectivity for narrow-band implementations. For wide-band implementations, however, inductive filter structures can exhibit a number of shortcomings. One of them is linked to the harmonic resonances (or higher order modes) of the basic resonators. The other is that the strong inductive couplings that are usually needed in wide-band designs, generally results in a degraded out-of-band performance of the filters. Many different techniques have indeed been explored in the technical literature, in order to improve the out-of-band performance. In [6], for instance, an integrated band-pass and band-reject filters in rectangular waveguide have been discussed in order to reduce, or suppress, the second harmonic of the filter. Also, in [7] an evanescent-mode filter has been designed with dielectric resonators in order to obtain a good spurious-free band. Other solutions have been discussed in [8] and [9], where the change in width of the resonators, and the use of stepped-impedance resonators (SIRs) are exploited in the design of rectangular waveguide filters with improved out-of-band performance. In addition, a non-uniform inductive filter with different resonator widths has also been proposed in [10], with the objective of improving the spurious-free stop band. Furthermore, in [11] an inductive bandpass filter was designed and implemented using non-uniform coupling window thicknesses, and resonators of different widths in order to further increase the level of spurious rejection. Recently, a new technique for rectangular waveguide inductive bandpass filters have been proposed in [12], where the coupling windows have been arranged in a particular configuration, with the objective to attenuate the high-order modes and improve the out-of-band response. However, all the contributions discussed so far are applicable only to narrow-band filter structures.

More recently, several papers have discussed the use of capacitive irises in band-pass filters [13], [14]. This is because band-pass filter with capacitive couplings (or *irises*) naturally provide a wide spurious free region above the pass-band. However, problems linked to the use of capacitive irises, are the appearance of unwanted resonances below the filter pass-band and, possibly, high power limitations. An additional example of the use of capacitive structures is shown in [15], where low-pass structures (capacitive shunt coupling) are used in the resonator with the objective of improving the stop-band attenuation.

One additional possibility is to design band-pass filters using hybrid couplings, that is, both capacitive and inductive irises. Recently, two contributions, namely [16] and [17], have demonstrated the use of stepped impedance resonators (SIRs) in conjunction with capacitive and inductive coupling irises (hybrid filter) in order to improve the out-of-band performance. The structures discussed in [16] and [17], do provide a wide spurious-free region above the filter pass-band

This work has been supported by Ministerio de Ciencia e Innovación (Spanish Government) under R&D project PID2019-103982RB-C41 and by Generalitat Valenciana under Santiago Grisolia grant GRISOLIA/2017/073.

J.F. Valencia Sullca, M. Guglielmi, S. Cogollos and V.E. Boria, are with the Departamento de Comunicaciones, iTEAM Group, Universitat Politècnica de València, E-46022 Valencia, Spain (e-mails: joavasu2@teleco.upv.es, marco.guglielmi@iteam.upv.es, sancobo@dcom.upv.es, vboria@dcom.upv.es).

implementing an important reduction of the strength of the harmonic resonances. But this improvement comes with an expensive manufacturing process and a rather complex design procedure.

Another very popular technique that can be used to improve both the out-of-band performance and the the filter selectivity is the introduction of transmission zeros (TZs) in the filter transfer function. This is traditionally achieved either with the use of cross-couplings between non-adjacent resonators, or with the use of extracted pole implementations, as discussed in [18]. Yet another solution has been discussed in [19], where higher order mode interactions in an inductive filter are exploited to generate transmission zeros in the out-of-band response of the filter. Furthermore, in [20] and [21] hybrid folded rectangular waveguide filters were proposed to obtain filter responses with TZs that can be located both above and below of the pass-band in a very wide frequency range. Also, in [22] a new capacitive obstacle in a rectangular waveguide structure was proposed to implement TZs. More recently, a contribution has shown how the out-of-band performance and selectivity of hybrid wide-band filters can be further improved by using, at the same time, a staircase configuration and E-plane T-junctions with shorted stubs [23]. However, in [23] the authors discuss only preliminary results based on simulations, without any measurement data.

In this context, therefore, the objective of this paper is to significantly extend the results presented in [23]. In particular, the additional topics discussed with respect to [23] are:

- The use of E-plane T-junctions, and E-plane folded structures to improve both the out-of-band response and the filter selectivity.
- Several hybrid staircase filters are also discussed, leading gradually to a final solution that has a very good performance and that is also very easy to manufacture.
- The analysis of the sensitivity to manufacturing errors in order to select the most appropriate manufacturing process.
- A multipaction analysis clearly showing that the hardware discussed is indeed suitable for space applications involving high power.
- A detailed study of the effects of the high order modes in the out-of-band response of the filter, including possible solutions to reduce their negative effects.

Finally, in addition to theory, we also discuss the comparison between the simulated and measured performance of an optimal hybrid staircase filter structure showing very good agreement, thereby fully validating both the new filter topology and the design procedure.

II. Filter Specifications

All filter designs normally start with a set of requirements that must be satisfied. In the context of this paper we will use the filter requirements shown in Table I. The objective of our filter design is to satisfy the requirements in Table I and, at the same time, to extend as much as possible the spurious-free frequency range above the pass-band. It is important to note that the above specifications have been already used in [17].

TABLE I
Electrical specifications for all the filters designed.

Parameter	Requirement
Bandwidth	$BW = 1410$ MHZ
In-band return loss	$RL > 20$ dB
Center frequency	$f_0 = 11$ GHz
Guide-wavelength fractional bandwidth	$\mathcal{W}_\lambda = 20$ %
Stopband rejection	> 50 dB
Waveguide WR-90	$a = 22.86$ mm $b = 10.16$ mm

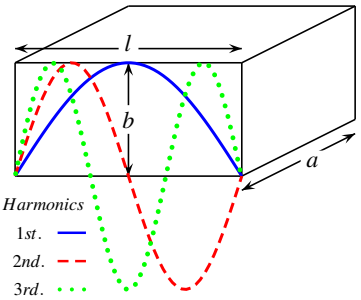

Fig. 1. The resonant modes of a rectangular waveguide cavity.

We will use them again in the remainder of this paper in order to compare the improvement obtained with the new filter structure that we propose.

III. Hybrid Staircase Filters

The objective of this section is to describe a new class of rectangular waveguide filters with inherent harmonic rejection capability. The basic idea is to couple resonators to each other in a way that prevents coupling of the higher order resonances.

A similar concept has already been proposed in [12] in the context of narrow-band filters coupled with inductive apertures. In this paper we propose instead to use capacitive coupling apertures. This change has two important consequences. The first is that capacitive irises can provide substantially higher values of coupling, with respect to inductive windows, even if the height b of the iris is relatively small. The second is that the small b results in a substantially stronger decoupling of the higher order resonances.

A. Basic staircase

To illustrate the basic concept behind the staircase configuration, we show in Fig. 1 the electric field distribution of first three resonant modes of a rectangular waveguide cavity of width a, height b and length l. As we can see in Fig. 1, the higher order resonances have alternating maximum and zero intensity values along the length l of the resonator. As a consequence, if we place a capacitive coupling aperture in the broad wall (top or bottom) of the waveguide in a location close to the electric field maximum of a higher order mode, we can very effectively reduce the coupling between higher order resonances. The application of this simple concept results into

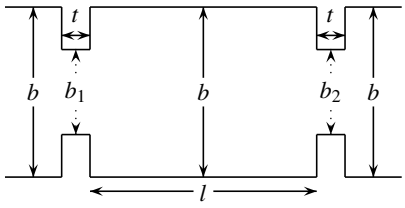

Fig. 2. Geometry of a resonator coupled with capacitive couplings in the front and end walls (side view).

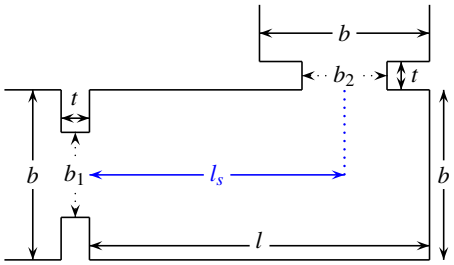

Fig. 3. Geometry of a staircase resonator with capacitive couplings (side view).

the *staircase* filter structure that is the main subject of this paper.

To better illustrate this concept, we first look at a resonator with capacitive couplings in the front and end walls, as shown in Fig. 2. Next, we show the geometry of a resonator with a staircase configuration (see Fig. 3). For this staircase configuration, if the coupling irises are opened on the top wall of the resonator at $l_s = l/2$, the resonators will not be coupled to each other. This is due to the fact that the first resonance shows a maximum of electric field in the middle of the resonator. A better iris location is $l_s = 3l/4$, where the second resonance has a maximum. With this choice, the first resonance will be coupled, while the coupling strength of the second resonance will be strongly decreased.

To show the effect of this choice, we now design a four-pole capacitive filter with bandwidth $BW = 720$ MHz. Fig. 4 shows the structure of this filter (filter 1). Next, we have designed a capacitive staircase filter (filter 2) using the concept shown in Fig. 3, where the capacitive irises are located on the broad wall of the waveguide at $l_s = 3l/4$, as we can see in Fig. 5.

Fig. 6 shows a comparison of the simulated behavior of

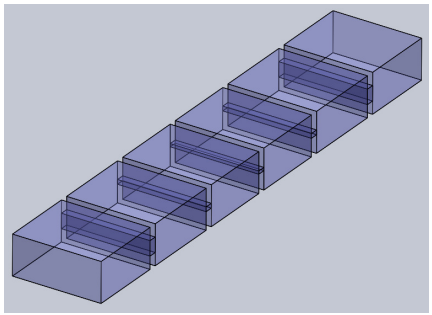

Fig. 4. Structure of the capacitive filter with $BW = 720$ MHz.

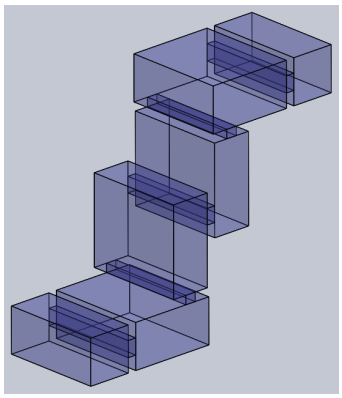

Fig. 5. Structure of the capacitive staircase filter with $BW = 720$ MHz.

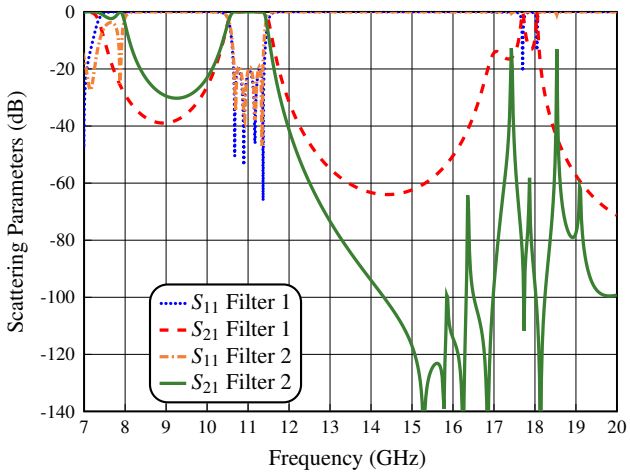

Fig. 6. Simulated performance of the capacitive reference filter (filter 1) and capacitive staircase filter (filter 2) with $BW = 720$ MHz.

the structures of Fig. 4 (filter 1) and Fig. 5 (filter 2). The performances shown in Fig. 6 have been obtained with the commercial tool FEST3D (v.2020 by AuroraSAT, now with Dassault Systèmes).

As we can see, filter 1 has a spurious (harmonic) response at about 17 GHz, which is due to the second resonance (TE_{102}). By contrast, filter 2 shows a substantial reduction and attenuation of the second harmonic, with spikes reaching about -15 dB at 17.4 and 18.5 GHz, respectively. However, the response of both filters below the pass-band shows a spurious response due to the use of capacitive irises.

Next, we explore the effect of the staircase configuration for wider bandwidths ($BW = 1410$ MHz and $\mathcal{W}_\lambda = 20$ %). Fig. 7 and Fig. 8 show the structures of an in line eight-pole capacitive filter (as a reference) and of an eight-pole capacitive staircase filter, respectively. Fig. 9 shows the comparison of the simulated behavior of the two structures. As we can see, the second resonance has been reduced to about -15 dB. However, below the pass-band the filter shows a spurious response above -30 dB, which is a significant degradation.

We can therefore conclude that the use of the staircase configuration in capacitive filters, for both narrow- and wide-band implementation, does show an important reduction of the harmonic resonances. However, in Fig. 9 we can also see that

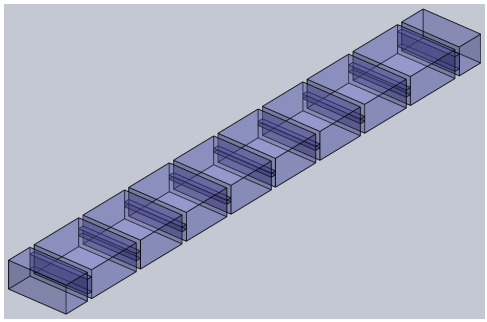

Fig. 7. Structure of the capacitive filter with $BW = 1410$ MHz.

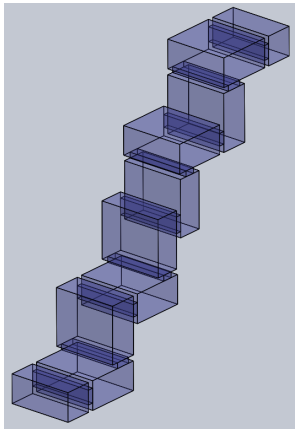

Fig. 8. Structure of the capacitive staircase filter with $BW = 1410$ MHz.

below the pass-band there is a significant spurious response. In the next section, we explore the use of hybrid coupling structures in order to address this issue.

B. Hybrid Staircase Filter

As already mentioned, hybrid structures have been successfully used in the past for the design of wide-band microwave filters. The basic concept is to use a number of inductive irises in the center of the filter to obtain a significant improvement

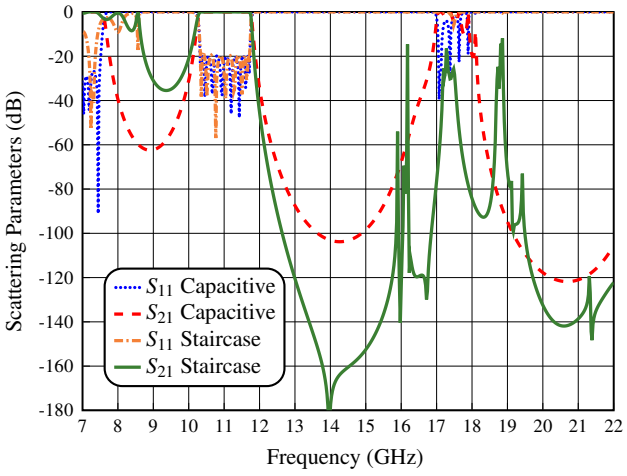

Fig. 9. Simulated performance of the capacitive reference filter and capacitive staircase filter with $BW = 1410$ MHz.

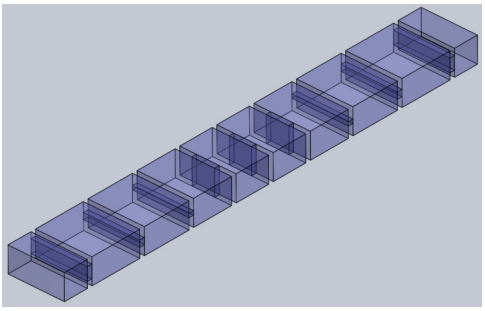

Fig. 10. Structure of the hybrid eight-pole filter with $BW = 1410$ MHz.

TABLE II
POSITION OF THE FIRST THREE RESONATORS FOR EACH STAIRCASE CONFIGURATION.

Type	Resonator 1	Resonator 2	Resonator 3
Staircase 1	Horizontal	Vertical	Horizontal
Staircase 2	Horizontal	Vertical	Vertical
Staircase 3	Horizontal	Horizontal	Horizontal
Staircase 4	Horizontal	Horizontal	Vertical

of the rejection below the pass-band. Similarly to what we have done in the previous section, we now design a reference eight-pole in-line filter, which satisfies the specifications of Table I with all capacitive coupling windows, except for the two central cavities that are coupled with the three inductive apertures (see Fig. 10).

In addition to the basic staircase configuration, there are also several possible variations that could be effectively used to further improve the out-of-band performance. In this context, therefore, we now explore different possible configurations for the first three resonators. Table II shows the different staircase configurations that can be obtained by changing the orientation of the first three resonators. In addition to the cavity orientation, we can also create different topologies by changing the location of the capacitive irises. Table III shows a number of possible iris locations. As we can see from Tables II and III, there are indeed many possible configurations. In our research, we have studied all of them in detail but, for the sake of space, we report in this paper only what we consider to be the best configuration, which turns out to be second staircase

TABLE III
LOCATION OF THE CAPACITIVE IRISES FOR EACH TOPOLOGY.

Type	Topology 1	Topology 2	Topology 3	Topology 4
Staircase 1	$l_{s_1} = l_1/4$ $l_{s_2} = l_2/4$	$l_{s_1} = 3l_1/4$ $l_{s_2} = l_2/4$	$l_{s_1} = 3l_1/4$ $l_{s_2} = 3l_2/4$	$l_{s_1} = l_1/4$ $l_{s_2} = 3l_2/4$
Staircase 2	$l_{s_1} = l_1/4$ $l_{s_2} = l_2/4$ $l_{s_3} = l_3/4$	$l_{s_1} = 3l_1/4$ $l_{s_2} = l_2/4$ $l_{s_3} = l_3/4$	$l_{s_1} = 3l_1/4$ $l_{s_2} = 3l_2/4$ $l_{s_3} = l_3/4$	$l_{s_1} = l_1/4$ $l_{s_2} = 3l_2/4$ $l_{s_3} = l_3/4$
Staircase 3	$l_{s_1} = l_1/4$ $l_{s_{2a}} = l_2/4$ $l_{s_{2b}} = l_2/4$ $l_{s_3} = l_3/4$	$l_{s_1} = 3l_1/4$ $l_{s_{2a}} = l_2/4$ $l_{s_{2b}} = l_2/4$ $l_{s_3} = l_3/4$	$l_{s_1} = 3l_1/4$ $l_{s_{2a}} = l_2/4$ $l_{s_{2b}} = 3l_2/4$ $l_{s_3} = l_3/4$	$l_{s_1} = l_1/4$ $l_{s_{2a}} = l_2/4$ $l_{s_{2b}} = 3l_2/4$ $l_{s_3} = l_3/4$
Staircase 4	$l_{s_1} = l_1/4$ $l_{s_{2a}} = l_2/4$ $l_{s_{2b}} = l_2/4$	$l_{s_1} = 3l_1/4$ $l_{s_{2a}} = l_2/4$ $l_{s_{2b}} = l_2/4$	$l_{s_1} = 3l_1/4$ $l_{s_{2a}} = l_2/4$ $l_{s_{2b}} = 3l_2/4$	$l_{s_1} = l_1/4$ $l_{s_{2a}} = l_2/4$ $l_{s_{2b}} = 3l_2/4$

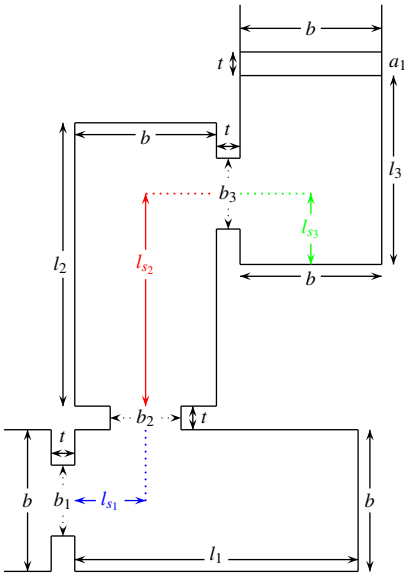

Fig. 11. Geometry of the three-resonator of the second staircase configuration with the capacitive coupling apertures located at $l_{s_1} = l_1/4$, $l_{s_2} = 3l_2/4$ and $l_{s_3} = l_3/4$ respectively, from the resonator input.

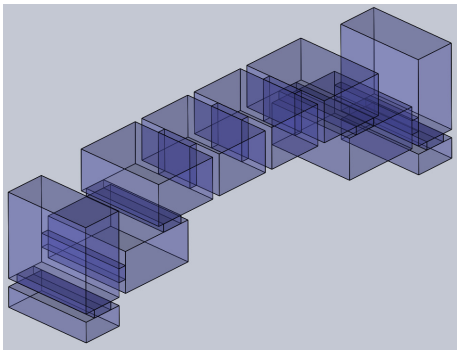

Fig. 12. Structure of the hybrid staircase filter of the topology 4.

configuration with the coupling irises arranged according to the fourth iris topology. Fig. 11 shows the geometry that we propose to use. The central section of the filter remains as shown in Fig. 10.

Fig. 12 shows the structure of the complete hybrid staircase filter. Fig. 13 shows a comparison of the simulated behavior of the reference in-line hybrid filter (hybrid), and the one in Fig. 12.

As we can see, we now have a significant reduction and attenuation of the second harmonic pass-band. The attenuation below the pass-band has also been increased. In addition, the structure generates TZs at 8 and 14 GHz. However, a spike has appeared reaching -50 dB just before 8.0 GHz.

We conclude that the implementation of the staircase configuration has shown an important improvement in the out-of-band response.

IV. E-PLANE T-JUNCTION MANIFOLD CONNECTION

In the previous sections we have designed filter structures with standard capacitive input and output couplings. A further improvement of the filter performance can be obtained using

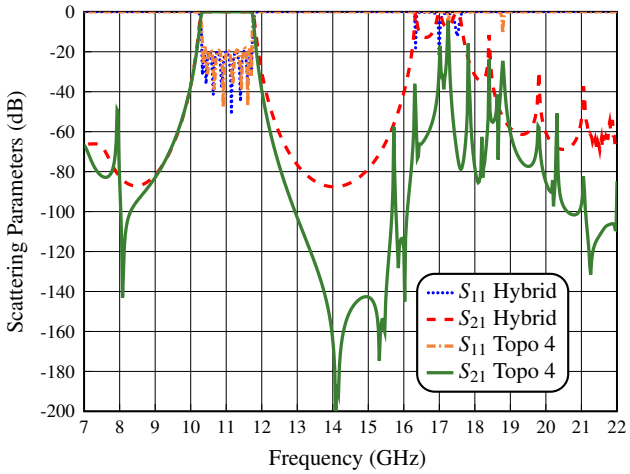

Fig. 13. Simulated performance of the hybrid reference filter (Hybrid) and hybrid staircase filter of the topology 4 (topo 4).

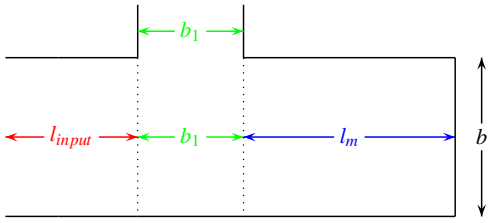

Fig. 14. Geometry of a simple E-plane manifold conection.

manifold connections, based on E-plane T-junctions, to generate additional TZs. It is, in fact, well-known that the short-circuited stubs used in a manifold connection generate TZs. To illustrate this concept, we show in Fig. 14 and Fig. 15 the geometry and the simulated performance of a simple manifold connection.

As we can see, the manifold connection generates a TZ below the filter pass-band, and another TZ above the pass-band. The specific location of the TZs depends on the length of the stub l_m. Therefore, if we change the length of the stub

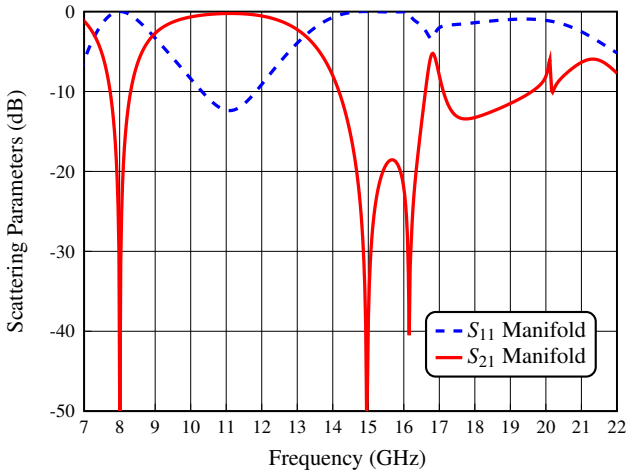

Fig. 15. Simulated performance of the manifold connection with a stub of length $l_m = \lambda/2 - b/2$.

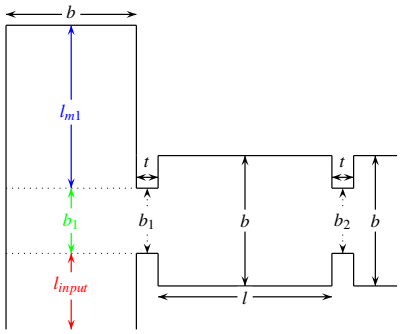

Fig. 16. Geometry of the E-plane T-junction in the input (or output) ports of a rectangular waveguide filter with capacitive couplings.

we can move the location of the TZs. We therefore propose to take advantage of this feature by using manifold connections both in the input and in the output ports of our filter. Fig. 16 shows the resulting (input and output ports) geometry.

An effective procedure that can be used to position the TZs in the wanted frequency location is as follows:

1) Design the waveguide filter with capacitive coupling in the input and output ports.
2) Add the manifold connection to both the input and the output ports of the filter.
3) To locate the TZ to the left of the pass-band, use a stub length approximately equal to $l_{m1} \approx \lambda/2 - b/2 - b_1/4$, where λ is the guide wavelength evaluated at the center frequency, b is the height of the rectangular waveguide and b_1 is the height of capacitive window in the input port of the filter.
4) To locate the TZ to the right of the pass-band, use a stub length approximately equal to $l_{m1} \approx \lambda/2 - b/2 + b_1/2$, where b_1 is the capacitive coupling in the output port of the filter.
5) Adjust by optimization the input and output irises to recover the desired filter performance.
6) Finally, fine tune by optimization the dimensions l_{m1} and b_1 in both the input and output ports, in order to produce the two TZs at desired frequency locations.

It is important to note, however, that there is a limitation with respect to the proximity of the TZ to the pass-band edge. We have, in fact, noted that, as the TZ gets closer to the pass-band, the capacitive coupling iris needs to be larger in order to recover the desired filter performance. As a consequence, the limit is reached when the coupling iris has the same height of the resonator to which it is connected. On the other hand, a reduction of the bandwidth of the filter, allows to move the TZ closer to the edge of the filter passband.

Following this design procedure, we have obtained the structure shown in Fig. 17. The simulated performance is shown in Fig. 18. As we can see, the addition of the manifold configuration produces a further improvement both in the selectivity and in the attenuation of the harmonics. This last filter has spurious response below -50 dB with a spike reaching -20 dB at 16.55 GHz.

We can therefore conclude that the combination of the staircase configuration with the manifold connection results in an important improvement of both the out-of-band response and the selectivity of the hybrid filters.

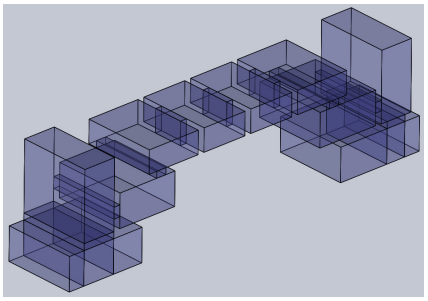

Fig. 17. Structure of the hybrid staircase filter of the topology 4 with manifold input-output connections.

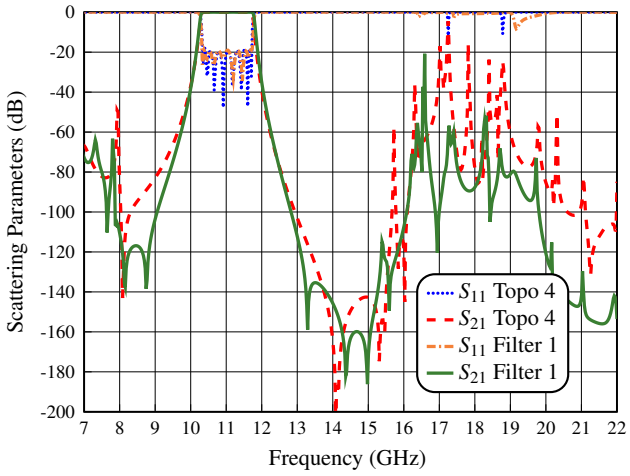

Fig. 18. Simulated performance of the hybrid staircase filter (topo 4) and hybrid staircase with manifold connections (filter 1).

V. E-PLANE FOLDED HYBRID FILTER

To further improve the attenuation of the harmonics in our filter, we explore in this section the possibility of folding the inductive part of the structure (see Fig. 19). In this context, we have explored in our research several possible folding configurations. Table IV shows the different folding possibilities that can be obtained by changing the orientation of the fourth resonator, and the inductive irises (a_1 and a_2) of the central inductive section of the filter. It is important to mention that the central section of the filter is symmetrical, for that reason, the length of the fourth and fifth resonator, and the width of the first and third inductive irises (a_1 and a_3) are equal.

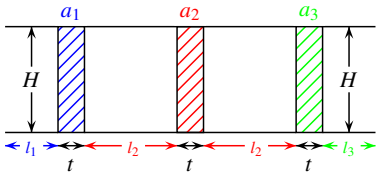

Fig. 19. Geometry of the central section of the filter in-line with inductive couplings (side view).

TABLE IV
POSITION OF THE FOURTH RESONATOR AND THE INDUCTIVE IRISES OF THE INDUCTIVE SECTION FOR EACH FOLDING CONFIGURATION.

Config.	Iris 1 (a_1)	Resonator 4	Iris 2 (a_2)
In-line	Horizontal	Horizontal	Horizontal
Folded 1	Horizontal	Horizontal	Vertical
Folded 2	Horizontal	Vertical	Horizontal
Folded 3	Horizontal	Vertical	Vertical
Folded 4	Vertical	Horizontal	Horizontal
Folded 5	Vertical	Horizontal	Vertical
Folded 6	Vertical	Vertical	Horizontal
Folded 7	Vertical	Vertical	Vertical

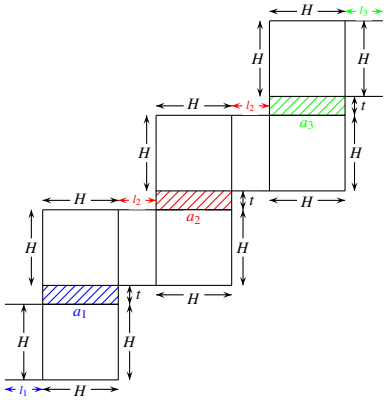

Fig. 20. Geometry of the E-plane folded 5.

In our research, we have studied in detail all of the possibilities. For the sake of space, however, we discuss in this paper only what we consider to be the best result, which turns out to be the fifth configuration. Fig. 20 shows the geometry that we propose to implement in the inductive part of the filter. Fig. 21 shows the resulting hybrid structure. Fig. 22 shows a comparison of the simulated behavior of the structures of Fig. 17 (filter 1) and Fig. 21 (folded 5).

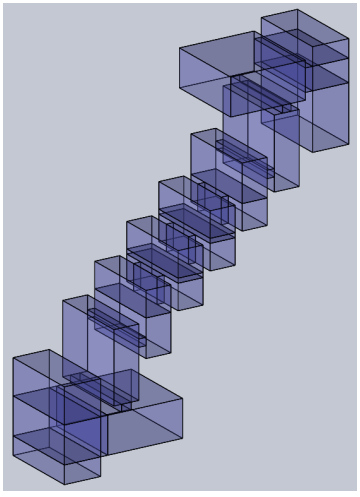

Fig. 21. Structure of the hybrid staircase with manifold inputs, and folded central section (folded 5).

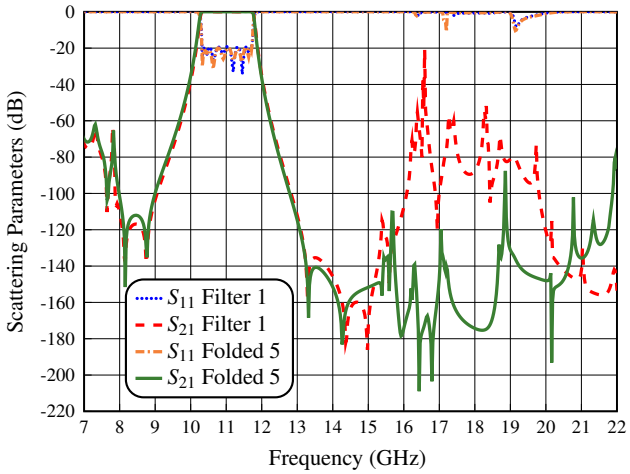

Fig. 22. Simulated performance of the hybrid staircase filter with manifold connections (filter 1) compared to the performance of the filter 1 with folded 5.

As we can see, folding the central section results in a further improvement of the out-of-band response in comparison with filter 1, namely, we now have a spurious response below -80 dB from 15 to 22 GHz. This is indeed an important improvement.

We can therefore conclude that folding the inductive part of the hybrid staircase filter further improves the reduction and the attenuation of harmonics resonance.

VI. THE PROTOTYPE

The filter structure that we have designed so far, has a very good out of band performance. However, the structure can not be fabricated *as is* because in all simulations we have used FEST3D in a fast but low accuracy setting. Furthermore, even if we could fabricate the structure as is, it could be a very expensive process because we have used *ideal* cavities with sharp 90 degree corners. What we now need, therefore, is a structure that is simulated with a very high precision, and that takes into account real manufacturing details.

The high accuracy design has been carried out following a combination of [24], and the well-known Aggressive Space Mapping (ASM) procedure [25] which requires the use of two separate electromagnetic simulations. The first one is carried out using FEST3D, with a fast but low accuracy setting (LA). The second is carried our using CST (v.2020, CST GmbH, now with Dassault Systèmes), which is a high accuracy (HA) but time-consuming simulator. Another important point is that all sharp concave corners have been replaced with rounded corners with a radius equal to $r = 1.1$ mm. The objective of this change is to reduce the manufacturing cost.

The final structure that we have obtained is shown in Fig. 23. Fig. 24 shows the comparison of the simulated performances obtained with FEST3D LA and CST. As we can see, the agreement is generally very good, except on the high frequency end where we can see a significant difference in the peak levels of the spurious responses. This is due to the fact that not enough higher order modes have been included explicitly in the LA simulations carried out with FEST3D LA.

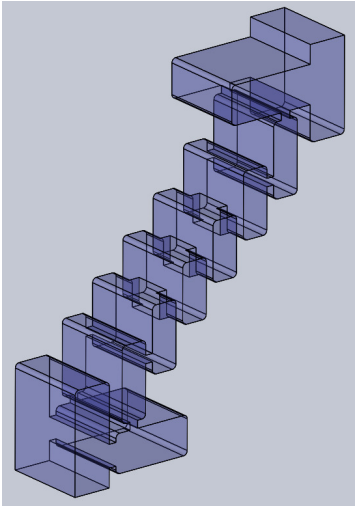

Fig. 23. Structure of the hybrid staircase filter with manifold inputs, and folded central section (folded 5) designed with a radius equal to $r = 1.1$ mm.

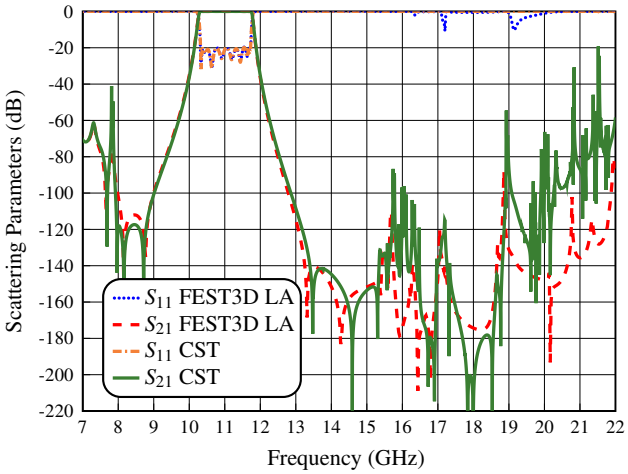

Fig. 24. Simulated performance of the hybrid staircase filter with manifold inputs, and folded central section (folded 5) using FEST3D LA and CST.

It is important to mention that we have considered up to 16 accessible modes in our simulations for low accuracy and 100 accessible modes for high accuracy. As a further validation, we have simulated the same structure with FEST3D HA. Fig. 25 shows the comparison of the simulated performances obtained with FEST3D HA and CST. As we can see, the agreement with the CST simulations is generally very good.

In any case, the high accuracy CST simulation shows a very good out-of-band response, with spurious below -50 dB from 15 to 22 GHz, and with spikes reaching -30 and -20 dB at 20.85 and 21.50 GHz, respectively (see Fig. 24).

Table V shows the final values for all dimensions of the filter. The dimensions are given up to the center of the filter. This is because the central (inductive) part is symmetrical, however, dimensions are given for the asymmetric parts of the structure. The thickness of the windows is t, and all resonators have the same width as the input waveguide.

To conclude this section, we have compared the performance of the filter discussed in this paper with the hybrid

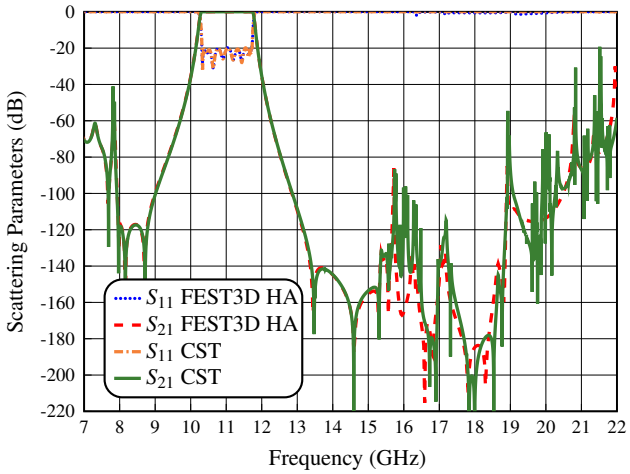

Fig. 25. Simulated performance of the hybrid staircase filter with manifold inputs, and folded central section (folded 5) using FEST3D HA and CST.

TABLE V
PHYSICAL DIMENSIONS FOR THE E-PLANE FOLDED HYBRID STAIRCASE FILTER WITH MANIFOLD CONNECTIONS.

Section Type	Dimensions (mm)
Input Waveguide	$a = 22.86$ $b = 10.16$ $L_{input} = L_{output} = 25$
Manifold T-junction 1-2	$a = 22.86$ $b = 10.16$ $l_{m1} = 9.660$ $l_{m2} = 15.750$
Capacitive window 1-6	$a = 22.86$ $b_1 = 10.16$ $b_6 = 6.026$ $t = 2$
Resonator 1-8	$H_1 = 10.16$ $L_1 = 21.294$ $H_8 = 10.16$ $L_8 = 21.213$
Capacitive window 2-5	$a = 22.86$ $b_2 = 2.557$ $b_5 = 2.277$ $t = 2$
Resonator 2-7	$H_2 = 7.00$ $L_2 = 19.420$ $H_7 = 7.00$ $L_7 = 19.659$
Capacitive window 3-4	$a = 22.86$ $b_3 = 2.110$ $b_4 = 2.110$ $t = 2$
Resonator 3-6	$H_3 = 7.000$ $L_3 = 17.379$ $H_6 = 7.000$ $L_6 = 17.379$
Inductive window 1-3	$a_1 = a_3 = 10.461$ $b = 7.000$ $t = 2$
Resonator 4-5	$H_4 = 7.000$ $L_4 = 15.505$ $H_5 = 7.000$ $L_5 = 15.505$
Inductive window 2	$a_2 = 9.858$ $b = 7.000$ $t = 2$

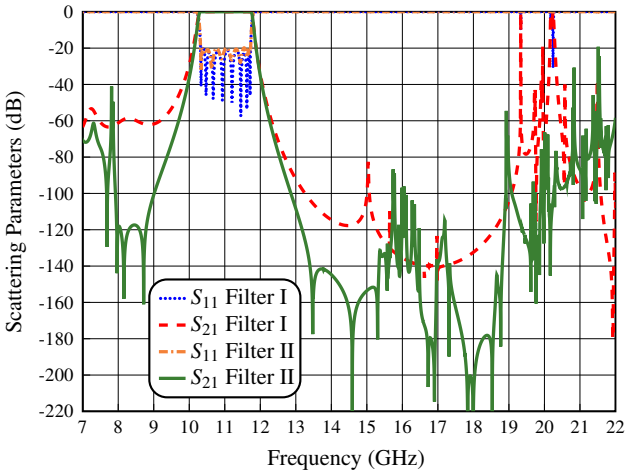

Fig. 26. Simulated performance of the E-plane folded hybrid SIR filter (filter I), and the E-plane folded hybrid staircase filter with manifold connections (filter II) using CST.

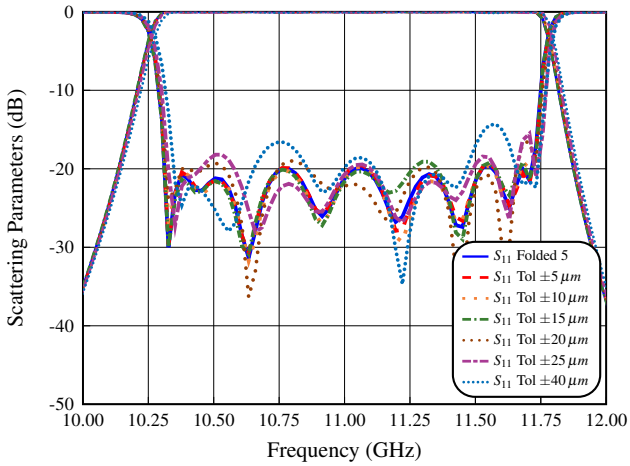

Fig. 27. Tolerance analysis of the hybrid staircase filter folded 5.

TABLE VI
RESULTS OF THE TOLERANCE ANALYSIS.

Filter Type	Yield of the Structures					
Tolerance	5 μm	10 μm	15 μm	20 μm	25 μm	40 μm
Folded 5	94 %	72 %	38 %	18 %	12 %	2 %

TABLE VII
HIGH POWER ANALYSIS OF THE HYBRID STAIRCASE FILTER FOLDED 5.

Structure	Power of the structure		
Frequency	$f_1 = 10.30$ GHz	$f_2 = 11.00$ GHz	$f_3 = 11.73$ GHz
b_3	5093 W	3531 W	1179 W
a_1	3718 W	21374 W	21124 W
a_2	4281 W	24748 W	17374 W

SIR filter (filter I) discussed in [17]. The results are shown in Fig 26. Both structures have been simulated in the commercial tool CST. As we can clearly see, the out-of-band response and the selectivity of filter II have been significantly improved with respect to filter I. Furthermore, the filter structure discussed in this paper is significantly simpler than the one discussed in [17].

VII. YIELD ANALYSIS

The filter structure that we discuss in this paper has been designed without including tuning elements. It is therefore important to perform a yield analysis. For this purpose, a random error with a Gaussian distribution has been added to the filter dimensions. This sensitivity analysis has been done using FEST3D. Different values of the standard deviation have also been used, namely, $\pm$ 5, $\pm$ 10, $\pm$ 15, $\pm$ 20, $\pm$ 25 and $\pm$ 40 μm. Furthermore, since the filter has been designed with a return loss of 20 dB, the threshold value for the yield estimation has been set to 18 dB. Table VI shows a summary of the results obtained.

Fig. 27 shows a number of simulations, including random errors. It is interesting to note that, from both the simulations and the results in Table VI, we can clearly conclude that with manufacturing errors between 5 and 10 μm, it should be possible to obtain an acceptable yield value.

VIII. HIGH POWER ANALYSIS

Another feature which is of great importance for space applications is the multipactor behavior of the filter [26]. We have therefore carried out a number of simulations in order to identify the power (Watts) where the multipactor effect can be initiated. In our simulations we have concentrated our attention on the central section of the filter due to the small dimensions of the irises (b_3, a_1 and a_2). Furthermore, the simulations have been performed at the frequencies where the group delay shows a maximum in the response of filter (f_1 and f_3) and at the centre frequency (f_2). The simulations have been carried out using FEST3D for the EM fields, and SPARK3D for the multipaction prediction, with the following set of parameters:

1) Initial power: 500 W
2) Maximum power: 1 MW
3) Growth factor of the power: 10^2
4) Frequencies of simulation: f_1, f_2 and f_3
5) Initial number of electrons: 10000

Table VII shows the power thresholds that we have obtained. As expected, the capacitive window (b_3) shows the lowest power threshold at 11.73 GHz with 1179 W. Finally, in Fig. 28 we show the values obtained for each simulation in this capacitive window.

The power level obtained is fully consistent with the levels currently used in the majority of space applications.

IX. MEASUREMENTS

The prototype discussed in the previous sections has been manufactured in a clam shell configuration using a combination of standard milling and spark erosion (see Fig. 29). It is important to note that the use of spark erosion is mandatory because of the small dimensions of the capacitive irises in the structure of filter, namely, b_3 and b_4. However, since most of the filter is manufactured with standard milling, the use of the more expensive spark erosion process for the irises

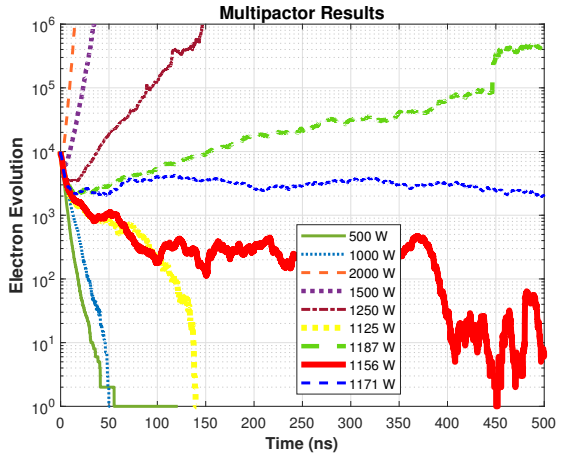

Fig. 28. Multipactor simulation with discharges for the capacitive window b_3 at 11.73 GHz.

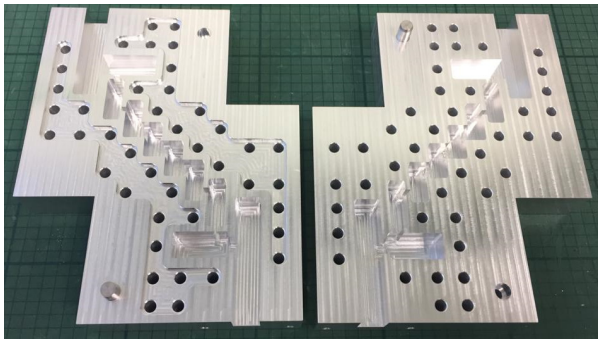

Fig. 29. Manufactured prototype in aluminum (no silver plating).

has the only effect of increasing very marginally the total manufacturing cost. The comparison between measured and simulated in-band and out-of-band responses are shown in Fig. 30 and Fig. 31, respectively.

Fig. 31 shows the electrical response in the stopband, in a wide frequency range. To produce this figure, we have used four standard waveguide calibrations, namely WR-90, WR-75, WR-62 and WR-51. The method used for the calibrations is TRL (True, Reflection and Line). The noise floor in each calibration was about -70 dB.

As we can see, the in-band performance is centered at 11 GHz, the 8 reflection zeros of the filter are clearly visible, and the agreement with the simulation is excellent. There is also a good agreement between simulation and measurement in the out-of-band response. However, there is a spike reaching -50 dB at about 16.15 GHz. The spike is probably due to manufacturing errors. It is important to mention that the manufacturing error has been kept below 10 microns for all the curved corners, and below 5 microns for all other filter elements. The filter performance that has been obtained is indeed excellent, and is in full agreement with the results of the yield analysis that we performed.

X. High Order Modes Effects

It is important to note at this point that, in the simulations we have used all modes generated internally within the structure

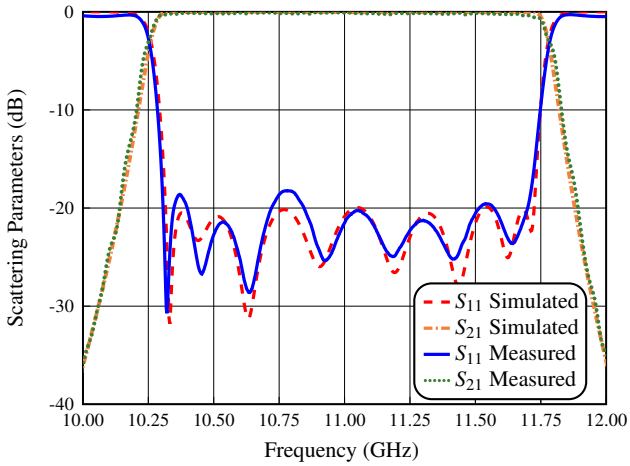

Fig. 30. Measurement of the in-band performance compared with the EM simulation (CST).

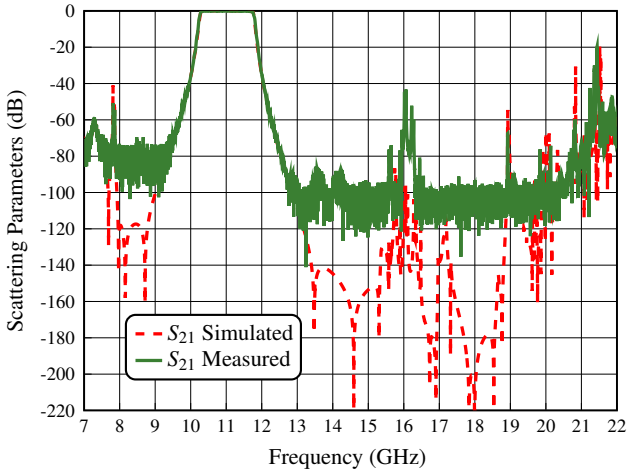

Fig. 31. Measurement of the out-of-band performance compared with the EM simulation (CST).

(100 accessible modes used to connect discontinuities and more than 3000 localized for their characterization [27]). However, as it is usually done in practice, the measured in- and out-of-band responses that we have discussed in the previous sections have been obtained measuring the response of the filter using only the fundamental TE_{10} mode excitation.

To complete our discussion, we will therefore study in this section the performance of our filter under higher order mode excitation. Table VIII shows the cut-off frequencies of the higher order modes that we have studied.

Fig. 32, Fig. 33, Fig. 34, and Fig. 35 show the comparison of the simulated performances of the filter excited with the higher order TE_{20}, TE_{11}, TM_{11}, TE_{30}, TE_{21} and TM_{21} modes obtained with FEST3D and CST, respectively. Our investigation indicates, however, that only two higher order modes need to be studied in detail, namely, the TE_{20} and TE_{30} modes. As we can see, Fig. 32 shows a spurious response at about 16 GHz, which is due to the TE_{20} mode. Furthermore, Fig. 34 shows a spurious response beginning at about 21.4 GHz with spikes reaching about -10 dB from 19.7 GHz, which is due to the TE_{30} mode.

TABLE VIII
THE HIGHER ORDER MODES CUT-OFF FREQUENCY.

Mode	Cut-off frequency
Waveguide WR-90	a =22.86 mm b =10.16 mm
TE_{10}	f_c =6.557 GHz
TE_{20}	f_c =13.114 GHz
TE_{01}	f_c =14.753 GHz
TE_{11}	f_c =16.145 GHz
TM_{11}	f_c =16.145 GHz
TE_{30}	f_c =19.671 GHz
TE_{21}	f_c =19.739 GHz
TM_{21}	f_c =19.739 GHz

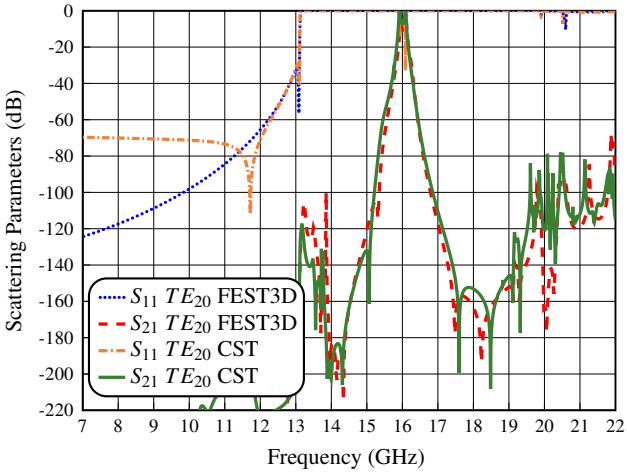

Fig. 32. Simulated performance of the hybrid staircase filter with manifold inputs, and folded central section (folded 5) for the higher order mode TE_{20} using FEST3D and CST.

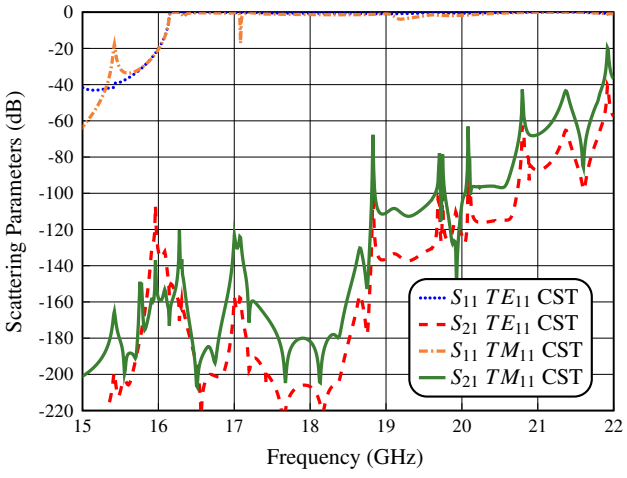

Fig. 33. Simulated performance of the hybrid staircase filter with manifold inputs, and folded central section (folded 5) for the higher order modes TE_{11} and TM_{11} using CST.

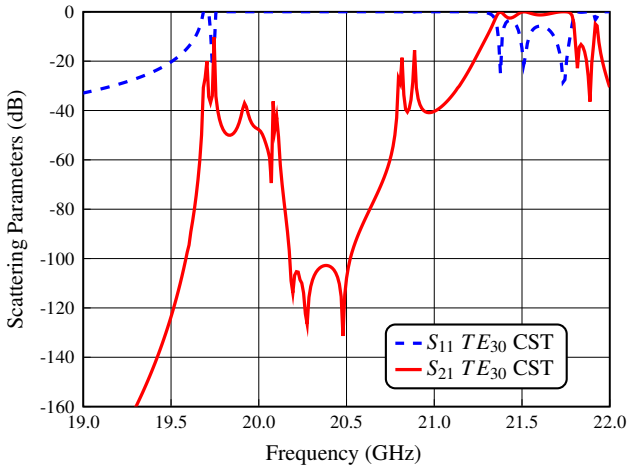

Fig. 34. Simulated performance of the hybrid staircase filter with manifold inputs, and folded central section (folded 5) for the higher order mode TE_{30} using CST.

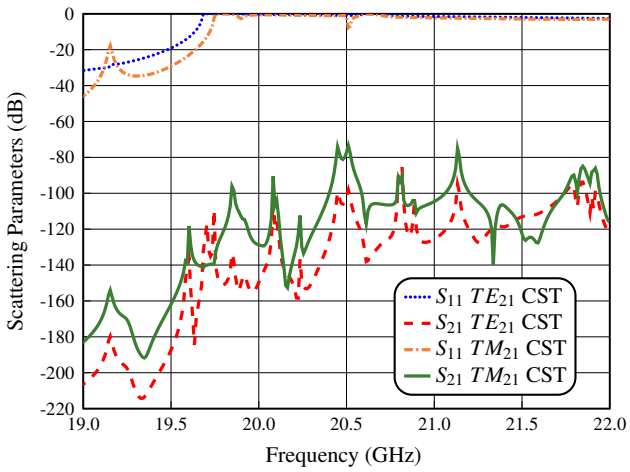

Fig. 35. Simulated performance of the hybrid staircase filter with manifold inputs, and folded central section (folded 5) for the higher order modes TE_{21} and TM_{21} using CST.

It is important to mention at this point that the measured out-of-band performance of our prototype shows slight differences with respect to the frequencies at which the higher order modes should be excited. This is probably due to manufacturing errors. In any case, the spurious responses degrade the response of the filter, and should therefore be eliminated.

The first consideration that is relevant in this context is the cause of the presence of the higher order modes in the input of the filter. In our measurement setup, the filter is connected to a vector network analyzer with two coaxial-to-waveguide transitions. These two transitions only allow the fundamental TE_{10} mode to be excited in the waveguide so that the TE_{20} is not present in the excitation. As result, no spurious signal is indeed observed. The use of coaxial cables and transitions to connect waveguide devices to each other is also very common in many actual applications. In that case, therefore, no particular action is necessary since the unwanted inputs are not present.

It is also true that in many real-life applications, rectan-

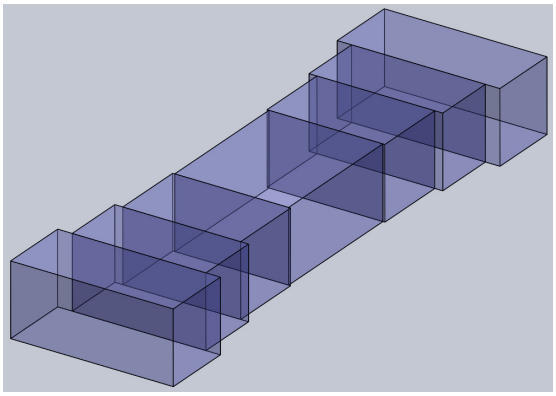

Fig. 36. Structure of the H-plane transformer composed of rectangular waveguide sections of smaller width.

gular waveguide filters are connected to other components using lengths of rectangular waveguide. It this second case, therefore, if higher order modes are generated in the payload before the filter, spurious signals can indeed be observed in the out-of-band response of the filter itself. However, the spurious responses generated by the higher order modes can be very easily suppressed connecting the device shown in Fig. 36 at the output of our filter. The device is a simple high-pass filter consisting of a H-plane transformer composed of rectangular waveguide section of smaller width. The length of the narrower waveguide can be chosen to obtain the needed level of spurious rejection. The beneficial effect of this high pass device is due to the fact that the higher order modes going through the filter are still below cut-off in the high pass section and, therefore, they are attenuated. This technique is well known and it is indeed of general value. In particular, the larger the distance between the cut-off of the waveguide used in the filter and the lower edge of the passband, the more effective is the suppression of the higher order modes of the filter. This is because, the width of the waveguide of the high-pass filter can be made significantly smaller than the width of the waveguide of the basic filter while keeping the cut-off of the high pass section just below the lower edge of the filter. The smaller the width of the waveguide of the high-pass filter, the higher the attenuation of the unwanted higher order modes. Table IX shows the final values for all dimensions of the high-pass filter. The dimensions are given up to the center of the device.

As we have already mentioned, our objective has been to reduce the effects of the TE_{20} and TE_{30} higher order modes in the out-of-band response of our filter. Fig. 37 and Fig. 38 show the comparison of the simulated performances of our filter, including the high-pass device, obtained with CST. As we can see, we now have spurious responses below -70 dB from 15 to 19.50 GHz, -50 dB from 19.50 to 21.25 GHz and -30 dB from 21.25 to 22 GHz, respectively. This is indeed an important improvement.

We have therefore clearly demonstrated that using the simple device shown in Fig. 36 we can effectively reduce the spurious responses generated by the higher order modes. Furthermore, it is important to note that the same effect can also be obtained by simply reducing the width of the central

TABLE IX
PHYSICAL DIMENSIONS FOR THE HIGH-PASS FILTER.

Section Type	Dimensions (mm)
Input Waveguide	$a = 22.86$ $b = 10.16$ $L_{input} = 10$
Section 1	$w_1 = 18.788$ $h_1 = 10.16$ $L_1 = 9.057$
Section 2	$w_2 = 16.556$ $h_2 = 10.16$ $L_2 = 10.604$
Section 3	$w_3 = 16.000$ $h_3 = 10.16$ $L_3 = 20.000$

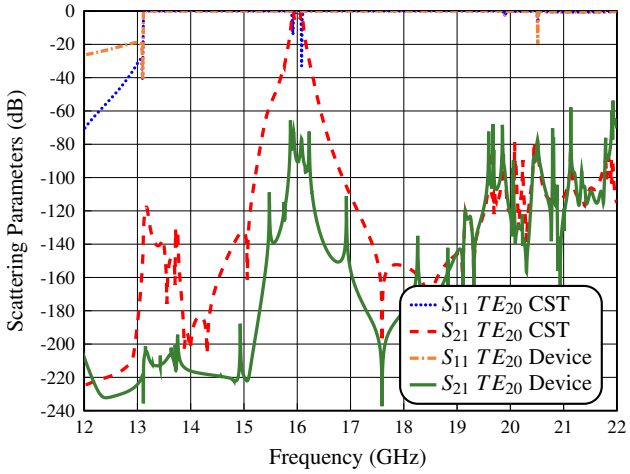

Fig. 37. Simulated performance (using CST) of our filter with TE_{20} excitation (TE_{20} CST) compared to the performance of the filter plus high-pass device (TE_{20} Device).

resonators in our filter, as we clearly show in the next section. This is, in fact, a very well-known technique to improve the out-of-band response of rectangular waveguide filters.

XI. Changing Central Resonator Width

The hybrid staircase filter discussed in the previous sections, has been designed with all resonators having the same width as the input waveguide. A significant improvement of the out-of-band response and, at the same time, a significant attenuation of the higher order modes can be obtained changing the width of the central resonators of the filter.

Fig. 39 shows the comparison of the simulated performances obtained with FEST3D HA and CST Studio Suite of the structure in Fig. 23 reducing the widths of the central resonators. As we can see, the agreement is very good. Also, simulations show a very good out-of-band response, with spurious below -50 dB from 13 to 22 GHz and a spike reaching -12.5 dB at 21.50 GHz.

Fig. 40 and Fig. 41 show the comparison of the simulated performances of our filter, including the reduction of the widths of the central resonators, obtained with CST for the

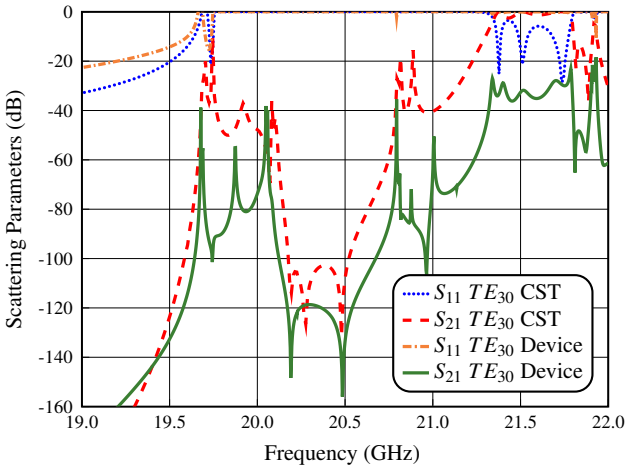

Fig. 38. Simulated performance (using CST) of our filter with TE_{30} excitation (TE_{30} CST) compared to the performance of the filter plus high-pass device (TE_{30} Device).

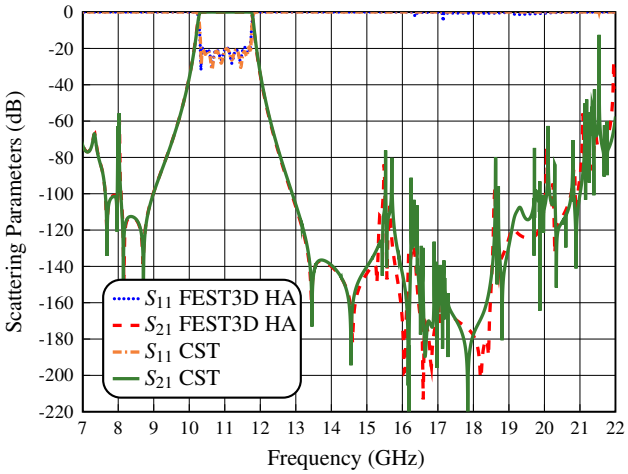

Fig. 39. Simulated performance of structure in Fig. 23 reducing the widths of the central resonators using FEST3D HA and CST.

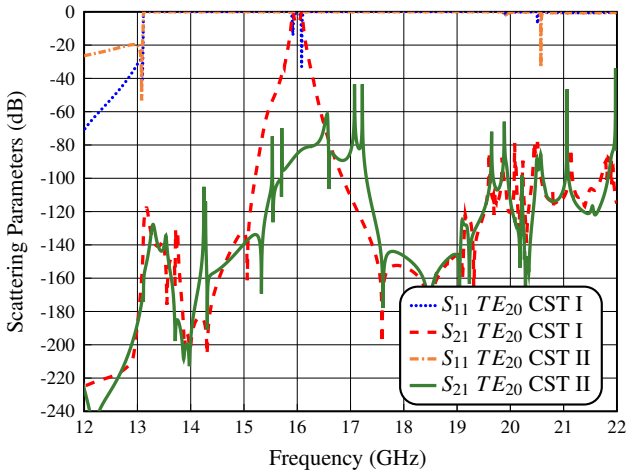

Fig. 40. Simulated performance (using CST) of the filter in Fig. 23 with TE_{20} excitation (TE_{20} CST I) compared to the performance of the filter in Fig. 23 reducing the widths of the central resonators (TE_{20} CST II).

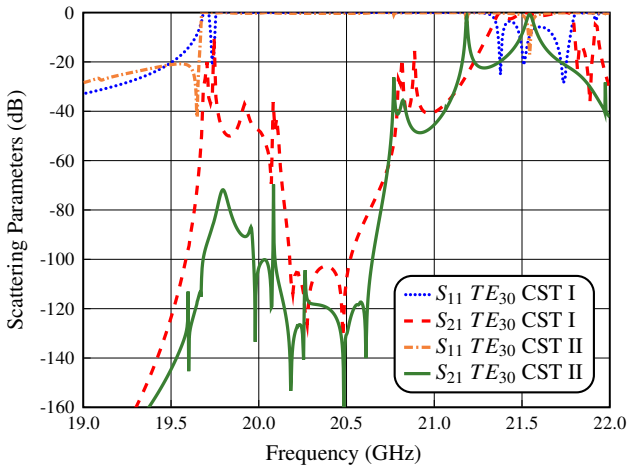

Fig. 41. Simulated performance (using CST) of the filter in Fig. 23 with TE_{30} excitation (TE_{30} CST I) compared to the performance of the filter in Fig. 23 reducing the widths of the central resonators (TE_{30} CST II).

higher order modes TE_{20} and TE_{30} . As we can see, we now have spurious responses below -50 dB from 15 to 19.50 GHz, -70 dB from 19.50 to 20.75 GHz and an important reduction of the spurious from 20.75 to 22 GHz, respectively. This is indeed an important improvement.

Table X shows the final values for all dimensions of the filter in Fig. 23 reducing the widths of the central resonators. The dimensions are given up to the center of the filter. This is because the central (inductive) part is symmetrical, however the dimensions of the asymmetric parts of the whole structure are also given. The thickness of the windows is t.

We can therefore conclude that reducing the width of the central resonators results in an important improvement in the out-of-band response of our filter and, at the same time, a reduction of the spurious responses generated by the higher order modes.

XII. Conclusion

In this paper, we have discussed the design of a wide-band filter based on a hybrid staircase configuration in rectangular waveguide, that has shown an important improvement in the out-of-band response and selectivity with respect to the state-of-the-art. Particular attention has also been devoted to the reduction of the negative effects due to the possible presence of higher order modes in the input of the filter. Furthermore, the structure that we discuss is very simple to manufacture using currently available machining techniques and does not require post-manufacturing adjustments (tuning). Detailed tolerance and high power analyses have also been carried out. In addition to theory, a prototype has also been manufactured and measured. The agreement between simulations and measurements has been found to be excellent, thereby fully validating both the filter structure and the design process.

References

[1] R.V. Snyder, "Filter design for modern communication systems," in *2012 Asia Pacific Microwave Conference Proceedings*, Dec. 2012, pp. 673–675.

TABLE X
PHYSICAL DIMENSIONS FOR THE NEW E-PLANE FOLDED HYBRID STAIRCASE FILTER WITH MANIFOLD CONNECTIONS.

Section Type	Dimensions (mm)
Input Waveguide	$a = 22.86$ $b = 10.16$ $L_{input} = L_{output} = 5$
Manifold T-junction 1-2	$a = 22.86$ $b = 10.16$ $l_{m1} = 9.671$ $l_{m2} = 15.750$
Capacitive window 1-6	$a = 22.86$ $b_1 = 10.16$ $b_6 = 6.065$ $t = 2$
Resonator 1-8	$W_1 = 22.86$ $W_8 = 22.86$ $H_1 = 10.16$ $L_1 = 21.334$ $H_8 = 10.16$ $L_8 = 21.322$
Capacitive window 2-5	$a = 22.86$ $b_2 = 2.629$ $b_5 = 2.323$ $t = 2$
Resonator 2-7	$W_2 = 22.86$ $W_7 = 22.86$ $H_2 = 7.00$ $L_2 = 19.467$ $H_7 = 7.00$ $L_7 = 19.726$
Capacitive window 3-4	$a = 21.50$ $b_3 = 2.098$ $b_4 = 2.098$ $t = 2$
Resonator 3-6	$W_3 = 21.50$ $W_6 = 21.50$ $H_3 = 7.000$ $L_3 = 17.943$ $H_6 = 7.000$ $L_6 = 17.943$
Inductive window 1-3	$a_1 = a_3 = 10.604$ $b = 7.000$ $t = 2$
Resonator 4-5	$W_4 = 20.00$ $W_5 = 20.00$ $H_4 = 7.000$ $L_4 = 16.265$ $H_5 = 7.000$ $L_5 = 16.625$
Inductive window 2	$a_2 = 10.081$ $b = 7.000$ $t = 2$

[2] R.V. Snyder, A. Mortazawi, I. Hunter, S. Bastioli, G. Macchiarella, and K. Wu, "Present and future trends in filters and multiplexers," *IEEE Trans. Microw. Theory Techn.*, vol. 63, no. 10, pp. 3324–3360, Oct. 2015.

[3] I. Arregui *et al.*, "High-power low-pass harmonic waveguide filter with TE_{n0} -mode suppression," *IEEE Microw. Wireless Compon. Lett.*, vol. 22, no. 7, pp. 339–341, Jul. 2012.

[4] F. Teberio *et al.*, "Chirping techniques to maximize the power-handling capability of harmonic waveguide low-pass filters," *IEEE Trans. Microw. Theory Techn.*, vol. 64, no. 9, pp. 2814–2823, Sep. 2016.

[5] G.L. Matthaei, L. Young, and E.M.T. Jones, *Microwave Filters, Impedance-Matching Networks, and Coupling Structures*. Norwood, MA: Artech House, 1980.

[6] M. Guglielmi, "Accurate CAD of integrated band-pass and second harmonic band-reject microwave filters," in *1998 IEEE MTT-S International Microwave Symposium Digest (Cat. No.98CH36192)*, vol. 2, Jun. 1998, pp. 813–816 vol.2.

[7] V.E. Boria *et al.*, "Contributions to the analysis and design of all-inductive filters with dielectric resonators," in *33rd European Microwave Conference Proceedings (IEEE Cat. No.03EX723C)*, vol. 3, Oct. 2003, pp. 1247–1250 Vol.3.

[8] M. Morelli, I. Hunter, R. Parry, and V. Postoyalko, "Stop-band improvement of rectangular waveguide filters using different width resonators: selection of resonator widths," in *2001 IEEE MTT-S International Microwave Sympsoium Digest (Cat. No.01CH37157)*, vol. 3, May 2001, pp. 1623–1626 vol.3.

[9] ——, "Stopband performance improvement of rectangular waveguide filters using stepped-impedance resonators," *IEEE Trans. Microw. Theory Techn.*, vol. 50, no. 7, pp. 1657–1664, Jul. 2002.

[10] P. Soto, E. Tarín, V.E. Boria, C. Vicente, J. Gil, and B. Gimeno, "Accurate synthesis and design of wideband and inhomogeneous inductive waveguide filters," *IEEE Trans. Microw. Theory Techn.*, vol. 58, no. 8, pp. 2220–2230, Aug. 2010.

[11] J.M. Perez Escudero, D. Martinez Martinez, A. Pons Abenza, J.A. Lorente Acosta, A. Alvarez-Melcon, and M. Guglielmi, "Enhancing the spurious free range in inductive rectangular waveguide filters," in *2015 European Microwave Conference (EuMC)*, Sep. 2015, pp. 678–681.

[12] Q. Wu, F. Zhu, Y. Yang, and X. Shi, "An effective approach to suppressing the spurious mode in rectangular waveguide filters," *IEEE Microw. Wireless Compon. Lett.*, vol. 29, no. 11, pp. 703–705, Nov. 2019.

[13] S. Li, J. Fu, and X. Wu, "Analysis of high-power rectangular waveguide filter with capacitive coupling iris for satellite," in *2009 Asia-Pacific Power and Energy Engineering Conference*, Mar. 2009, pp. 1–4.

[14] ——, "Rectangular waveguide band pass filter with capacitive coupling iris," in *Progress in Electromagnetics Research Symposium 2008 (PIERS 2008)*, Mar. 2008, pp. 337–341.

[15] W. Menzel, A. Muller, and F. Bogelsack, "A capacitively coupled waveguide filter with wide stop-band," in *2003 33rd European Microwave Conference*, Oct. 2003, pp. 1239–1242.

[16] J. Valencia, M. Guglielmi, S. Cogollos, J. Vague, and V.E. Boria, "Enhancing the performance of stepped impedance resonator filters in rectangular waveguide," in *2017 47th European Microwave Conference (EuMC)*, Oct. 2017, pp. 989–992.

[17] J. Valencia, V.E. Boria, M. Guglielmi, and S. Cogollos, "Compact wideband hybrid filters in rectangular waveguide with enhanced out-of-band response," *IEEE Trans. Microw. Theory Techn.*, vol. 68, no. 1, pp. 87–101, Jan. 2020.

[18] R.J. Cameron, C.M. Kudsia, and R.R. Mansour, *Microwave Filters for Communication Systems: Fundamentals, Design and Applications*, 2nd ed. Hoboken, NJ, USA: John Wiley & Sons, 2018.

[19] M. Guglielmi, F. Montauti, L. Pellegrini, and P. Arcioni, "Implementing transmission zeros in inductive-window bandpass filters," *IEEE Trans. Microw. Theory Techn.*, vol. 43, no. 8, pp. 1911–1915, Aug. 1995.

[20] C. Carceller, P. Soto, V.E. Boria, M. Guglielmi, and D. Raboso, "New folded configuration of rectangular waveguide filters with asymmetrical transmission zeros," in *2014 44th European Microwave Conference*, Oct. 2014, pp. 183–186.

[21] C. Carceller, P. Soto, V.E. Boria, and M. Guglielmi, "Design of hybrid folded rectangular waveguide filters with transmission zeros below the passband," *IEEE Trans. Microw. Theory Techn.*, vol. 64, no. 2, pp. 475–485, Feb. 2016.

[22] ——, "Capacitive obstacle realizing multiple transmission zeros for in-line rectangular waveguide filters," *IEEE Microw. Wireless Compon. Lett.*, vol. 26, no. 10, pp. 795–797, Oct. 2016.

[23] J. Valencia, M. Guglielmi, S. Cogollos, and V.E. Boria, "Enhancing the out-of-band response of hybrid wide-band filters in rectangular waveguide," in *2020 50th European Microwave Conference (EuMC)*, Jan. 2021, pp. 747–750.

[24] M. Guglielmi and A.A. Melcon, "Novel design procedure for microwave filters," in *1993 23rd European Microwave Conference*, Sep. 1993, pp. 212–213.

[25] J.W. Bandler, R.M. Biernacki, R.H. Hemmers, and K. Madsen, "Electromagnetic optimization exploiting aggressive space mapping," *IEEE Trans. Microw. Theory Techn.*, vol. 43, no. 12, pp. 2874–2882, Dec. 1995.

[26] E. Sorolla *et al.*, "An analytical model to evaluate the radiated power spectrum of a multipactor discharge in a parallel-plate region," *IEEE Trans. Electron Devices*, vol. 55, no. 8, pp. 2252–2258, 2008.

[27] G. Conciauro, M. Guglielmi, and R. Sorrentino, *Advanced modal analysis*. Wiley, 2000.

Joaquin F. Valencia Sullca was born in Lima, Peru, on March 14, 1990. He received the degree in telecommunication engineering from the Universidad Nacional de Ingeniería (UNI), Lima, Peru, in 2013, the master degree in communication technologies, systems and networks from the Universitat Politècnica de València, Valencia, Spain, in 2016, where he is currently pursuing the Ph.D. degree in telecommunications with the iTEAM Group. His current research interests include the analysis and design of passive components, electromagnetic simulations, efficient design and optimizations of waveguide filters, and its applications.

Marco Guglielmi was born in Rome, Italy, on December 17, 1954. He received the degree "Laurea in Ingegneria Elettronica" in 1979 from the University of Rome "La Sapienza", Rome, Italy, where in 1980 he also attended the "Scuola di Specializzazione in Elettromagnetismo Applicato". In 1981 he was awarded a Fulbright Scholarship in Rome, Italy, and an HISP (Halsey International Scholarship Programme) from the University of Bridgeport, Bridgeport, Connecticut, USA, where in 1982 he obtained an MS Degree in Electrical Engineering. In 1986 he received a PhD degree in Electrophysics from the Polytechnic University, Brooklyn, New York, USA. From 1984 to 1986 he was Academic Associate at Polytechnic University, and from 1986 to 1988 he was Assistant Professor in the same institution. From 1988 to 1989 he was Assistant Professor at the New Jersey Institute of Technology, Newark, New Jersey, USA. In 1989 he joined the European Space Agency as a Senior Microwave Engineer in the RF System Division of the European Space Research and Technology Centre (ESTEC), Noordwijk, The Netherlands, where he was in charge of the development of microwave filters and electromagnetic simulation tools. In 2001 he was appointed Head of the Technology Strategy Section of ESTEC where he contributed to the development of management processes and tools for the formulation of a European strategy for Space Technology Research and Development. In 2014 Dr. Guglielmi retired from the European Space Agency and is currently holding the position of Invited Senior Researcher at the Polytechnic University of Valencia, Valencia, Spain. Dr. Guglielmi has been elevated to the grade of Fellow of the IEEE in January 2013 "For contributions to multimode equivalent networks and microwave filter design".

Santiago Cogollos was born in Valencia, Spain, on January 15, 1972. He received the degree in telecommunication engineering and the Ph. D. degree from the Universitat Politècnica de València (UPV), Valencia, Spain, in 1996 and 2002, respectively. In 2000 he joined the Communications Department of the Universitat Politècnica de València, where he was an Assistant Lecturer from 2000 to 2001, a Lecturer from 2001 to 2002, and became an Associate Professor in 2002. He has collaborated with the European Space Research and Technology Centre of the European Space Agency in the development of modal analysis tools for payload systems in satellites. In 2005 he held a post doctoral research position working in the area of new synthesis techniques in filter design at University of Waterloo, Waterloo, Ont., Canada. His current research interests include applied electromagnetics, mathematical methods for electromagnetic theory, analytical and numerical methods for the analysis of microwave structures, and design of waveguide components for space applications.

Vicente E. Boria (S'91-A'99-SM'02-F'18) was born in Valencia, Spain, on May 18, 1970. He received his "Ingeniero de Telecomunicación" degree (with first-class honors) and the "Doctor Ingeniero de Telecomunicación" degree from the Universidad Politécnica de Valencia, Valencia, Spain, in 1993 and 1997, respectively. In 1993 he joined the "Departamento de Comunicaciones", Universidad Politécnica de Valencia, where he has been Full Professor since 2003. In 1995 and 1996, he was holding a Spanish Trainee position with the European Space Research and Technology Centre, European Space Agency (ESTEC-ESA), Noordwijk, The Netherlands, where he was involved in the area of EM analysis and design of passive waveguide devices. He has authored or co-authored 10 chapters in technical textbooks, 180 papers in refereed international technical journals, and over 200 papers in international conference proceedings. His current research interests are focused on the analysis and automated design of passive components, left-handed and periodic structures, as well as on the simulation and measurement of power effects in passive waveguide systems. Dr. Boria has been a member of the IEEE Microwave Theory and Techniques Society (IEEE MTT-S) and the IEEE Antennas and Propagation Society (IEEE AP-S) since 1992. He is also member of the European Microwave Association (EuMA), and has been the Chair of the 48th European Microwave Conference held in Madrid, Spain. He acts as a regular reviewer of the most relevant IEEE and IET technical journals on his areas of interest. He has been Associate Editor of IEEE Microwave and Wireless Components Letters (2013-2018) and IET Electronics Letters (2015-2018). Presently, he serves as Subject Editor (Microwaves) of IET Electronics Letters, and as Editorial Board member of International Journal of RF and Microwave Computer-Aided Engineering. He is also member of the Technical Committees of the IEEE-MTT International Microwave Symposium and of the European Microwave Conference.